JOURNAL OF THERMOPHYSICS AND HEAT TRANSFER
Vol. 16, No. 3, July–September 2002

Distributions of Recovery Temperature on Flat Plate by Underexpanded Supersonic Impinging Jet

Byung Gi Kim,* Man Sun Yu,* Yong Il Cho,* and Hyung Hee Cho†
Yonsei University, Seoul 120-749, Republic of Korea

An experimental investigation has been conducted on the impingement of underexpanded, axisymmetric, and supersonic jets on a flat plate. The surface pressure and the adiabatic wall temperature distributions on the flat plate have been measured in detail at small nozzle-to-plate distances. The influences of the pressure ratio, the exit Mach number, the nozzle-to-plate distance, and the impinging angle have been considered. The results show that the surface pressure and the adiabatic wall temperature distributions on the flat plate for supersonic jet impingement are affected significantly by the nozzle-to-plate distance and the existence of a stagnation bubble in the central region.

Nomenclature

D_{ne} = nozzle exit diameter
L_{ps} = standoff distance of the plate shock (Fig. 4)
M_D = design Mach number at the nozzle exit plane
P_a = ambient pressure
P_C = pressure in the settling chamber
P_e = pressure at the nozzle exit plane
P_r = ratio of the nozzle exit pressure to the ambient pressure, P_e/P_a
R = radial distance from the center
r = recovery factor [Eq. (1)]
T_{aw} = adiabatic wall temperature
T_j^d = jet dynamic temperature
T_j^s = jet static temperature
T_j^0 = jet total temperature
Z = axial distance from the nozzle exit
Z_p = distance from the nozzle exit plane to the center of a plate
Z_S = distance from the nozzle exit plane to the normal shock (Fig. 4)
θ = angle between the nozzle axis and the plate

Introduction

WHEN a supersonic jet impinges on a solid surface, dynamic energy is converted to thermal energy, and a high temperature is induced on the surface. Therefore, severe aerodynamic and thermal loads can be produced on it.[1] Impingement of a supersonic jet on solid objects can be found in various situations, such as the launch of a rocket, the takeoff and landing of a vertical/short takeoff and landing aircraft, jet-engine exhaust impingement, the thrust vector control system of a solid rocket motor, and so on. It may be used for material testing of heat shields such as shuttle tiles. Supersonic jet impingement includes very complicated phenomena, with the presence of a multiple shock system that consists of the barrel shock, the plate shock, and the reflected shock, as well as the instability of a stagnation bubble.

Previous investigations have concentrated mainly on flow pattern, pressure distributions on the target surface, and visualization of shock wave structures using optical techniques for perpendicular[1–8] and inclined[9,10] impingement, whereas only a few results associated with heat transfer[4,11,12] have been reported.

The purpose of the present study is to obtain basic information on supersonic jet impingement on solid objects. An experimental investigation has been carried out on the impingement of axisymmetric, underexpanded, and supersonic jets on a flat plate, and the surface pressure and the adiabatic wall temperature distributions on a flat plate have been measured. In the present experiments, the ratio of the nozzle exit pressure to the ambient pressure, the Mach number at the nozzle exit, the nozzle-to-plate distance, and the angle between the nozzle axis and the plate (hereinafter referred to as an impinging angle) have been considered as the variables of interest.

Experimental Apparatus and Method

Two different nozzles are used in the present experiments: One is the convergent–divergent conical nozzle that has the divergence half angle of 15 deg (hereinafter referred to as a supersonic nozzle), and the other is the contoured convergent nozzle (hereinafter referred to as a sonic nozzle). The throat diameter of the supersonic nozzle is 10.0 mm, and the diameter of nozzle exit is 12.0 mm, which gives a design Mach number of 1.8 calculated from one-dimensional isentropic relations. The sonic nozzle has the exit diameter of 10.0 mm and a design Mach number of 1.0.

Figure 1 shows the schematic diagram of the experimental apparatus used for the present investigation. Air is compressed up to 150 kgf/cm^2 by a reciprocating compressor and passes through five stage air filters to remove moisture. It is then stored in three storage tanks. The compressed air is supplied to the settling chamber through regulators from the storage tanks. The nozzle, from which a jet issues, is mounted on the settling chamber.

The supplied air is heated with an electric heater and the total temperature of a jet is controlled to remain close to the ambient air temperature (within the difference of $\pm 0.5^\circ$C), to minimize the effect of entrainment of the ambient air with a different temperature.

The impingement plate for the adiabatic wall temperature measurement is made of phenolic, which is an insulation material ($k = 0.19$ W/m $\cdot\,^\circ$C) with a thickness of 10 mm. The back side of the plate is insulated with fiberglass ($k = 0.046$ W/m $\cdot\,^\circ$C) and Styrofoam® ($k = 0.028$ W/m $\cdot\,^\circ$C), which are 10 and 20 mm thick, respectively. The plate is instrumented with 37 T-type (copper–constantan) thermocouple junctions spaced 2.5 mm apart within 30 mm from the center in the radial direction, where significant variation of temperature is expected, and 5 mm apart outside the center region.

Another plate with four pressure taps is used for measurement of the surface pressure. The surface pressure is measured with a Druck pressure transducer (PMP4070) connected to each pressure tap.

Received 19 October 2001; revision received 3 February 2002; accepted for publication 4 February 2002.

*Graduate Student, School of Mechanical Engineering.
†Associate Professor, Department of Mechanical Engineering, 134, Shinchon-dong, Seodaemun-ku; hhcho@yonsei.ac.kr. Member AIAA.

Table 1 Experimental conditions

Mach number	Pressure ratio		Impinging angle	Nozzle-to-plate distance
M_D	$P_r(=P_e/P_a)$	P_0/P_a	θ, deg	Z_P/D_{ne}
1.0	1.5	2.84	90	0.5–1.5
1.8	1.5	8.62	90	0.5–3.0
1.8	1.5	8.62	75	1.0, 2.0, 3.0
1.8	1.5	8.62	60	1.0, 2.0, 3.0
1.8	1.5	8.62	45	2.0, 3.0
1.8	1.2	6.90	90	0.5–3.0

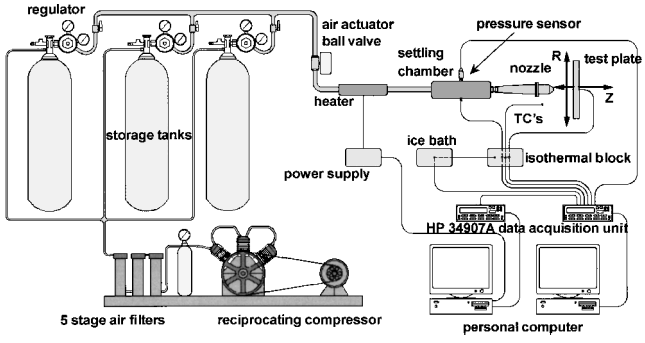

Fig. 1 Schematic diagram of experimental apparatus.

The test plates are mounted on a motorized linear motion system and can be moved both in the axial direction Z and in the radial direction R; therefore, precise adjustment of nozzle-to-plate distance and radial movement of pressure taps during the tests have been achieved.

The output signals from thermocouples and pressure transducers are scanned and acquired using Agilent 34970A data acquisition/switch units equipped with HP 34902A 16-channel multiplexer modules and stored in a personal computer.

The experiments have been conducted mainly for the case of $M_D = 1.8$, $P_r = 1.5$, and $\theta = 90$ deg, and the results are compared to those cases with variation in each parameter. The experimental conditions are summarized in Table 1 namely, the Mach numbers at the nozzle exit of 1.8 and 1.0, the ratios of the nozzle exit pressure to the ambient pressure of 1.2 and 1.5, the nozzle-to-plate distances from 0.5 to 3.0, and the impinging angles from 90 to 45 deg.

In addition, pitot pressure measurements are made along the axes of the freejets using a pitot tube of 1.0-mm o.d. tip. To visualize the structures of shock waves in the freejets and the impingement region, shadowgraphs are taken for several selected cases.

Results and Discussion

Pitot Survey for Freejets

Shadowgraphs of freejets issuing from the supersonic nozzle are presented in Fig. 2. Figure 2a is taken for the pressure ratio of 1.5, and Fig. 2b is for $P_r = 1.2$. The expansion waves from the nozzle lip reflect from the constant pressure jet boundary as compression waves and subsequently coalesce to form the barrel shock. The barrel shock terminates in a triple point Mach disk configuration. A region of subsonic flow bounded by a slip line is formed behind the Mach disk.[13]

Figures 2a and 2b show typical patterns of underexpanded supersonic jets. Comparing Figs. 2a and 2b reveals that the higher pressure ratio of 1.5 results in the larger Mach disk at the farther downstream location. The positions of the Mach disks measured from the shadowgraphs are approximately $1.3D_{ne}$ for $P_r = 1.2$ and $1.6D_{ne}$ for $P_r = 1.5$.

Figure 3 presents the results of pitot pressure measurements at the center of freejets and the central surface pressure on the perpendicular impingement plate for comparison. The measured pressure is normalized with respect to the pressure in the settling chamber. Downstream of the nozzle exit, the pitot pressure decreases as the axial distance increases due to the flow acceleration, and slight recompression occurs at $Z/D_{ne} = 1.1$, which is probably due

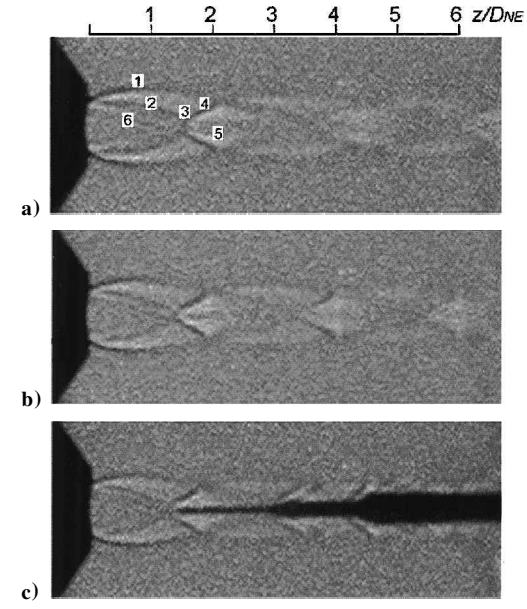

Fig. 2 Shadowgraphs of supersonic freejets: a) M_D = 1.8 and P_r = 1.5: 1, constant pressure boundary; 2, barrel shock; 3, Mach disk; 4, reflected shock; 5, slip line; and 6, nozzle shock; b) M_D = 1.8 and P_r = 1.2; and c) M_D = 1.8 and P_r = 1.2, the tip of a pitot probe at Z/D_{ne} = 1.42 (downstream of Mach disk).

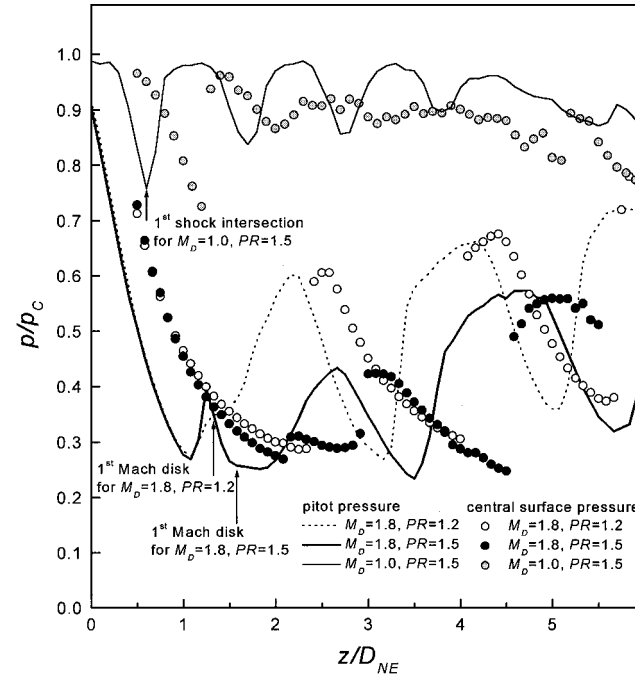

Fig. 3 Distributions of pitot pressure on the freejet centerline and the central surface pressure for a perpendicular plate.

to a nozzle shock generated immediately downstream of the nozzle throat. The experimental results, which confirm formation of an oblique shock in a conical nozzle, have been also reported by Back and Cuffel.[14] In the case of $P_r = 1.5$, there is the region of constant pitot pressure at $1.58 \le Z/D_{ne} \le 1.92$. This region corresponds to the subsonic core behind the Mach disk, as shown in Fig. 2a. Downstream of the subsonic core, the pressure rises again steeply due to the momentum transfer from the outer region of the slip line with high total pressure to the central part of the jet. When the flow in the vicinity of centerline is reaccelerated and becomes supersonic, the pitot pressure decreases again.

In the case of $P_r = 1.2$, the diameter of Mach disk is smaller than that for P_r of 1.5, and, consequently, the subsonic core behind the Mach disk is weakly formed. Therefore, the region of constant pitot pressure immediately downstream of the Mach disk (at $Z/D_{ne} \geq 1.33$) is not observed, and the slope of pitot pressure slightly decreases at that position. The downstream pressure repeats a decrease and increase due to alternate compression and expansion in the jet.

For $M_D = 1.0$ and $P_r = 1.5$, initial decrease of pitot pressure occurs until $Z/D_{ne} = 0.6$, where $P/P_C = 0.76$. This value is much higher than that for $M_D = 1.8$ ($P/P_C = 0.25$ at $Z/D_{ne} = 1.58$). This can be explained by the total pressure loss for $M_D = 1.0$ decreasing due to the lower upstream Mach number compared to that for $M_D = 1.8$. The pressure recovery owing to inward momentum transfer takes place up to $P/P_C = 0.98$, and this high-pressure recovery repeats until the fourth shock cell.

Considerable discrepancy is observed between the pitot pressure and the central surface pressure because the standoff distance of the bow shock formed in front of a pitot probe is less than that of the plate shock. Note that, as the shadowgraph result in Fig. 2c shows, the Mach disk seems not to be affected by a pitot probe placed in the subsonic core downstream of the Mach disk. On the contrary, the pattern of shock waves in a jet is changed significantly by insertion of a plate.

Perpendicular Jet Impingement

Figure 4 presents the distances from the nozzle exit to the normal shock and the standoff distances of the plate shock measured from the shadowgraph results.

At the small nozzle-to-plate distance, only one normal shock exists in front of the impingement plate. As the nozzle-to-plate distance increases, both Z_S and L_{ps} increase. At a certain position of impinging plate, an additional shock wave is formed upstream of the plate shock, and Z_S increases abruptly. As shown in Fig. 3, it corresponds to the position where the sudden rise of the central surface pressure occurs. In other words, the sudden pressure recovery, which takes place at $2.33 < Z_P/D_{ne} < 2.41$ for $P_r = 1.2$ and at $2.92 < Z_P/D_{ne} < 3.0$ for $P_r = 1.5$, results from the change of shock structure like that in front of the plate. The location of the newly formed shock wave, which is nearer to the nozzle exit, equals that of the Mach disk in the freejets.

Figure 5 shows shadowgraphs of a perpendicular impinging jet at selected nozzle-to-plate distances. The sudden rise of

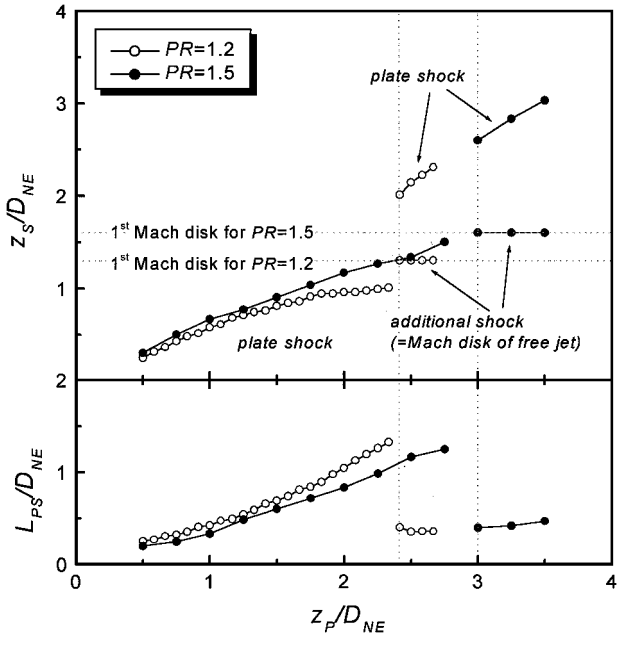

Fig. 4 Positions of shock waves and standoff distance of plate shocks for $M_D = 1.8$.

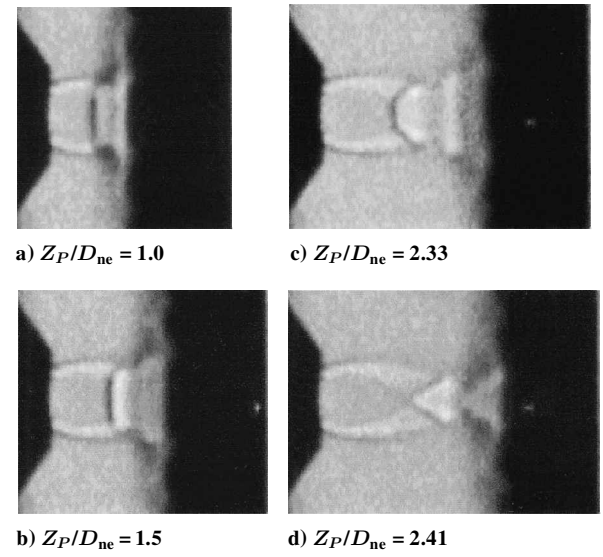

Fig. 5 Shadowgraphs of perpendicular jet impingement for $M_D = 1.8$, $P_r = 1.2$ with various nozzle-to-plate distances.

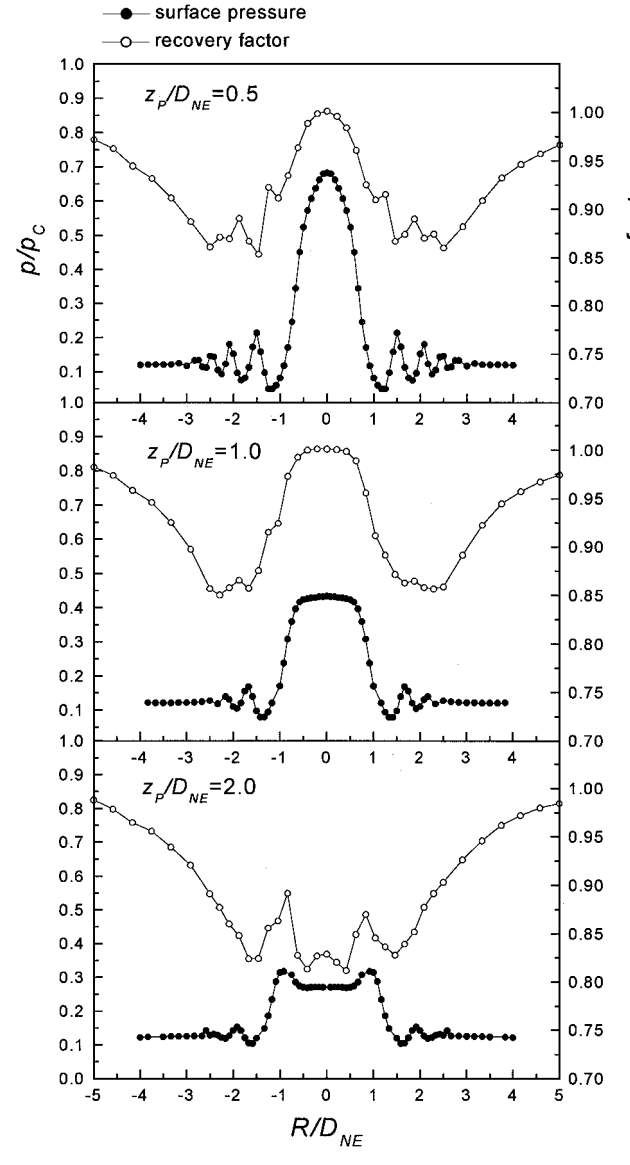

Fig. 6 Surface pressure and recovery factor for perpendicular impingement ($M_D = 1.8$ and $P_r = 1.5$) with various nozzle-to-plate distances.

central surface pressure mentioned earlier occurs between positions corresponding to Figs. 5c and 5d. It is shown that significantly different patterns of shock waves are induced by a slight change in plate location.

Figure 6 shows the distributions of surface pressure and the corresponding adiabatic wall temperature for $M_D = 1.8$ and $P_r = 1.5$ for several nozzle-to-plate distances. The adiabatic wall temperature measurements are presented in dimensionless form using a recovery factor. The definition of the recovery factor is as follows:

$$r = \frac{T_{\text{aw}} - T_j^s}{T_j^d} = 1 + \frac{T_{\text{aw}} - T_j^0}{T_j^d} \tag{1}$$

where

$$T_j^d = \frac{u_j^2}{2C_P} = \frac{[(\gamma - 1)/2]M^2}{1 + [(\gamma - 1)/2]M^2} T_j^0$$

The experimental uncertainties in recovery factor and pressure are calculated using the method of Kline and McClintock.[15] The

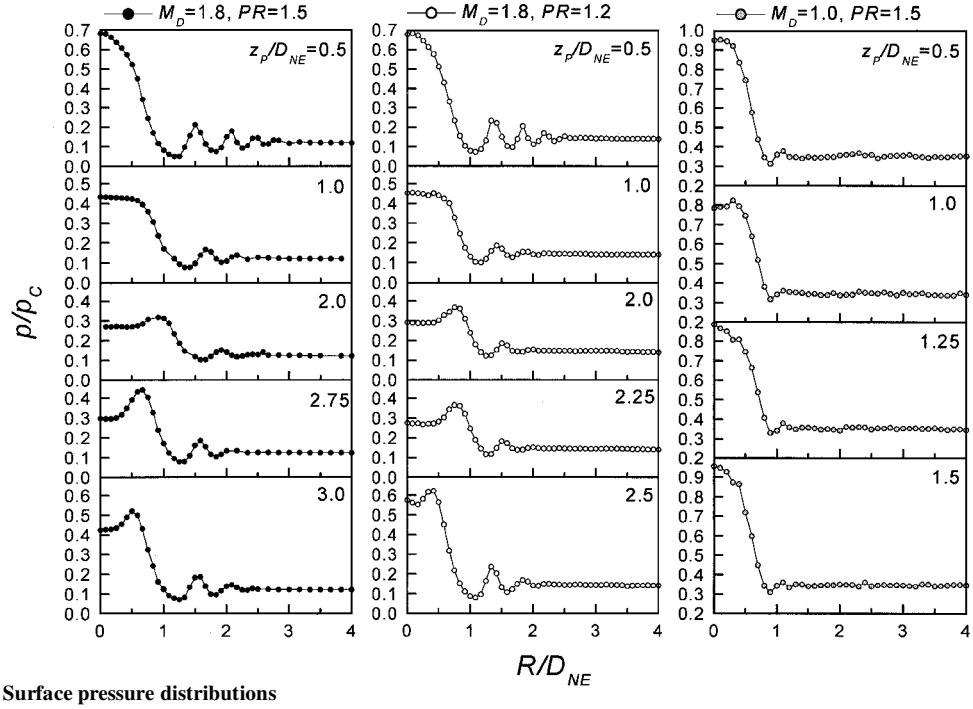

Surface pressure distributions

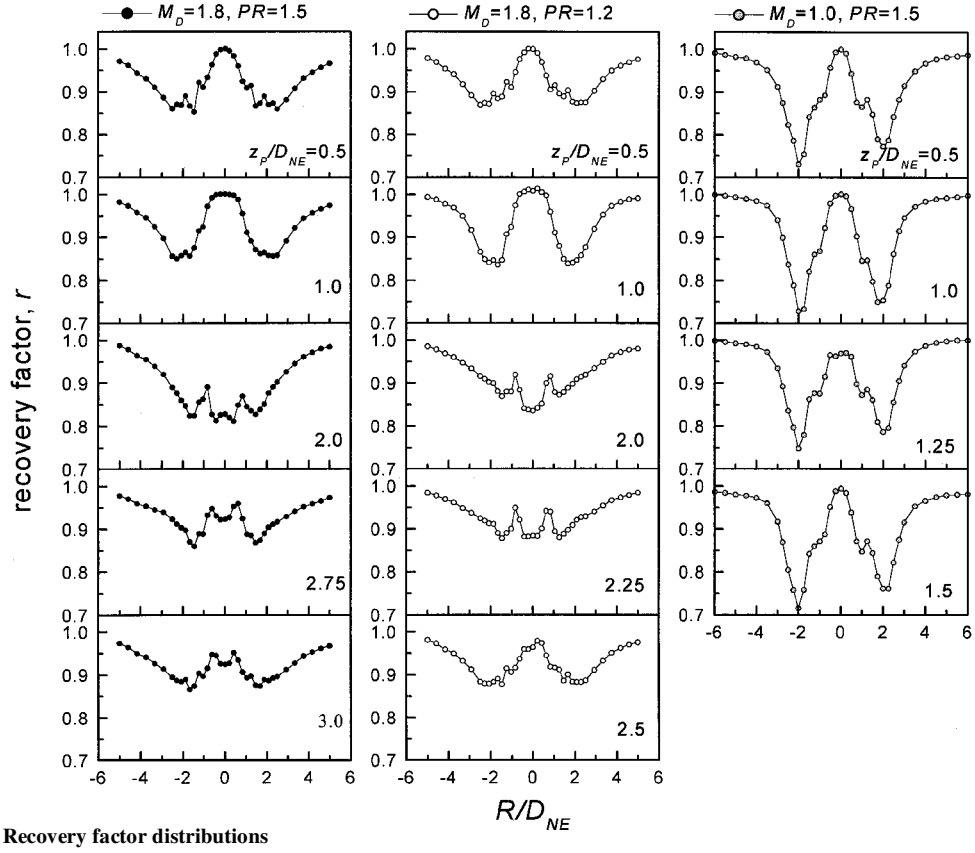

Recovery factor distributions

Fig. 7 Perpendicular jet impingement for various M_D and P_r.

uncertainties of the recovery factor and the surface pressure normalized with respect to the chamber pressure are within ±3.5 and ±2.1%, respectively, with a confidence level of 95%.

The surface pressure distribution has a maximum of $0.69P_C$ at the center and then decreases to the periphery at $Z_P/D_{ne} = 0.5$. The adiabatic wall temperature at this plate location has a maximum at the center and gradually decreases, but it is recovered up to the ambient temperature in the far outer region as the shear layer grows along the jet boundary.

The large valley of recovery temperature around the jet periphery seems to be due to the "vortex-induced cooling (energy separation)" that is discussed by Fox et al.[11] They showed that the secondary vortices generated near the plate surface, which are induced by the approach of the primary vortices formed at the nozzle lip, contribute to lowering the wall temperature in the annular region near the jet center when the plate is inserted at a small distance from the nozzle. The peripheral cooled region consistently observed from our recovery data can be explained by the total temperature separation due to this unsteady vortical structure.

Several pressure peaks occur in the wall jet region (at $R/D_{ne} > 1$) because compression and expansion occur alternately due to the reflection of expansion fans from the intersection of the jet edge and the reflected shock by the upper boundary of the wall jet and the plate in the wall jet region.[2,7]

The distribution of recovery factor also shows small peaks and valleys in this region. These peaks and valleys can be related to the total temperature separation due to vortical structure, which has a different cause from that mentioned earlier. When the expansion waves are reflected from the upper boundary of wall jet as strong compression waves, and they interact with the boundary layer in the wall jet region, the boundary-layer separation and the formation of vortices may occur locally. At these regions, the pressure gradient is adverse, and wall temperature is reduced locally by the total temperature separation due to the vortical structure. Consequently, the locations of the pressure peaks correspond to those of the recovery temperature valleys. The local peaks and valleys of recovery temperature like these can obviously be observed only at the very small nozzle-to-plate distance.

As the plate is moved farther from the nozzle exit to $Z_P/D_{ne} = 1.0$, the central pressure decreases to $0.43P_C$ due to the increased total pressure loss with increased upstream Mach number and is almost uniform within the central region ($R/D_{ne} \leq 0.5$), where the recovery factor also has a constant value of unity. The jagged profile of the surface pressure and the recovery factor at the wall jet region becomes less sharpened as nozzle-to-plate distance increases.

At $Z_P/D_{ne} = 2.0$, the surface pressure has a maximum at $R/D_{ne} \approx 1.0$, and such a peripheral maximum of the pressure suggests that recirculating flow (called a stagnation bubble) occurs in the central region, as reported previously.[1,5,6] The adiabatic wall temperature at $Z_P/D_{ne} = 2.0$ is significantly lowered in the central region, where the existence of a stagnation bubble is expected. Fox and Kurosaka[12] showed that the unsteady movement of the shock structure, influenced by the formation and movement of vortices, may cause energy separation, that is, central cooling in the supersonic freejet. The primary cause of cooling in the central region observed from the present result is due to shock-induced total temperature separation discussed by them.

However, the low-temperature recovery in the central region is observed for most of the cases that have their maximum pressure at the periphery in the present tests. Thus, it can be inferred that the stagnation bubble may also be relevant to the central cooling. The relation between the low-temperature recovery in the central region and the existence of a stagnation bubble cannot be estimated quantitatively at this stage. At the very least, if the fluid particles with lowered total temperature due to the shock–vortex interaction are trapped in a stagnation bubble for a relatively longer duration (than without a stagnation bubble), it can be said that the stagnation bubble contributes to the cooling in the central region.

Figure 7 shows surface pressure and recovery factor distributions as a function of nozzle-to-plate distance. The surface pressure and the adiabatic wall temperature distributions for $M_D = 1.8$ and $P_r = 1.2$ have sequential variations similar to those for $P_r = 1.5$, and there is a little difference due to the reduced length of first shock cell and higher pressure recovery, which are dependent on the degree of underexpansion. For the lower pressure ratio of 1.2, the nozzle-to-plate distance, where the sudden rise of central pressure after the first shock cell occurs, is reduced, and central pressure recovery is slightly higher, as shown in Fig. 3. The central pressure downstream of first shock cell is about 60% of chamber pressure for $P_r = 1.2$ but about 40% for $P_r = 1.5$.

From the results for $Z_P/D_{ne} \geq 2.0$, it seems that reduction in the recovery factor in the central region is somewhat dependent on the scale of the stagnation bubble: Where the radius of annular stagnation ring is larger, the recovery factor in the central region is much lower.

The results for $M_D = 1.0$ and $P_r = 1.5$ show the common feature of the cooling effect around the jet periphery compared to those for a higher Mach number of $M_D = 1.8$ with the same pressure ratio. However, unlike the former cases, the peripheral maximum of pressure is not observed, and no central cooled region appears regardless of the nozzle-to-plate distance.

Inclined Jet Impingement

For inclined jet impingement, the jet is not axisymmetric and surface phenomena have two-dimensional characteristics. However,

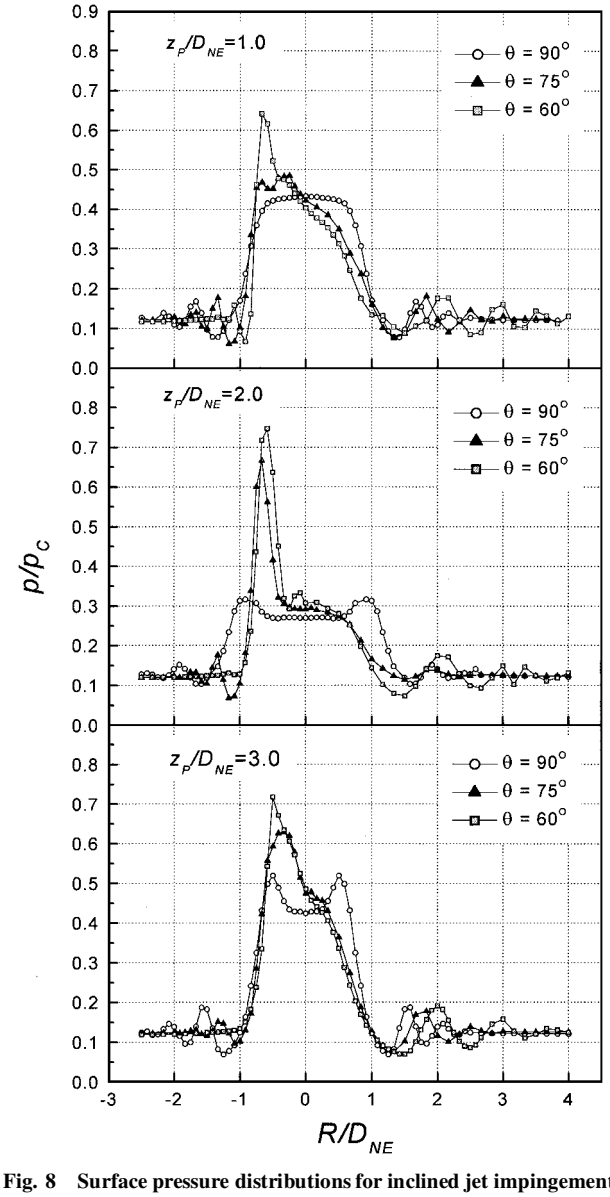

Fig. 8 Surface pressure distributions for inclined jet impingement.

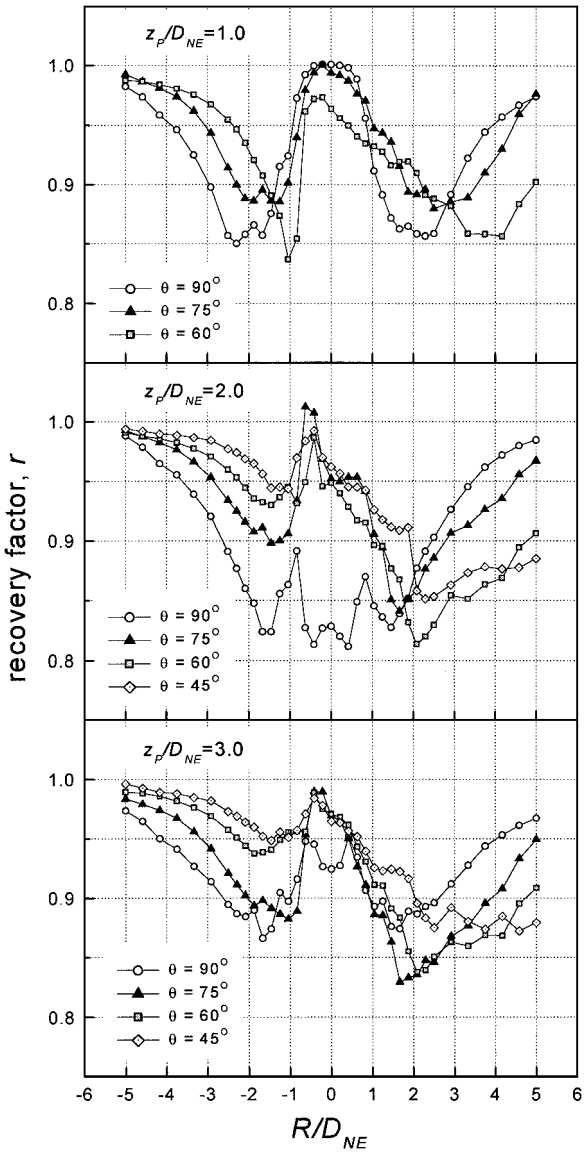

Fig. 9 Recovery factor distributions for inclined jet impingement.

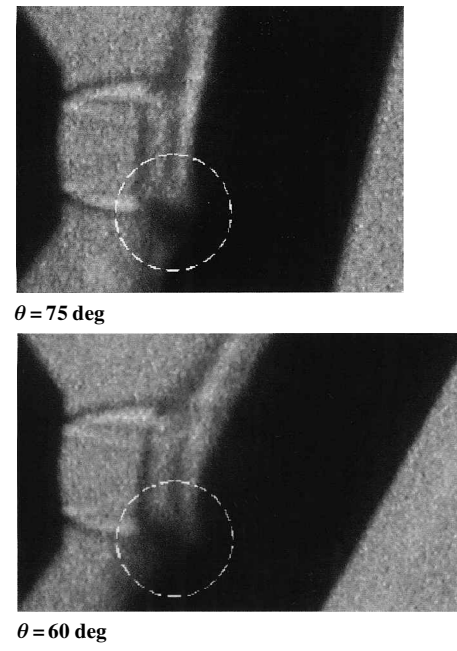

Fig. 10 Shadowgraphs of inclined jet impingement for M_D = 1.8, P_r = 1.5, and Z_P/D_{ne} = 1.0.

because main features are expected to be found on the plane of symmetry, the distributions of the surface pressure and the recovery temperature on it are measured and compared with the results for the perpendicular jet impingement. For the inclined jet impingement, the axial distance from the nozzle exit to the geometric center of a plate is denoted by Z_P.

Figure 8 presents surface pressure distributions for various impinging angles at the nozzle-to-plate distances of 1.0, 2,0 and 3.0. The recovery factor distributions are shown in Fig. 9. The exit Mach number M_D is 1.8 and pressure ratio P_r is 1.5 for all of the cases.

In the case of $Z_P/D_{ne} = 1.0$ and $\theta = 90$ deg, the surface pressure has a maximum of $0.43P_C$ at the center, but the peak pressure increases as the impinging angle decreases, and the peak location is moved slightly upward (in the negative R direction). The maximum pressure is $0.48P_C$ and $0.64P_C$ at $\theta = 75$ and 60 deg, respectively. The shadowgraph results in Fig. 10 show that the pressure peaks are located in the upper tail shock region. Lamont and Hunt[9] showed that the maximum pressure occurs in the upper tail shock region due to the movement of the stagnation streamline into the upper tail flow for inclined jet impingement. The upward pressure decreases abruptly to the level of the ambient pressure because the expansion fans are formed at the intersection of the tail shock and the jet edge. At $Z_P/D_{ne} = 2.0$ and 3.0, the peripheral pressure peaks occur for perpendicular jet impingement, but such a feature cannot be observed as the impinging angle decreases. This means that there is no stagnation bubble for the case of inclined jet impingement.

The location of the peak adiabatic wall temperature is also moved upward like that of the pressure as the impinging angle decreases, and its value is close to unity.

In the wall jet region, the recovery of temperature in the upward direction becomes faster as the impinging angle decreases, whereas recovery in the downward direction is retarded farther downstream. The wiggle of recovery factor, which seems to be related to complex reflection of shock and expansion waves by the upper boundary of the wall jet and the plate, is conspicuous in the downward region and changes sensitively with the impinging angles.

At $Z_P/D_{ne} = 2.0$ and 3.0, the recovery factor at the center of plate is over 0.95 for inclined cases when no stagnation bubble is expected from the pressure distributions, and it has a higher value than that for the perpendicular case. Therefore, it is supplementary evidence that the reduction of the recovery factor in the central region for the perpendicular impingement is influenced by the existence of a stagnation bubble.

Conclusions

An experimental investigation has been conducted on impingement of axisymmetric, underexpanded, supersonic jets on a flat plate. The surface pressure and adiabatic wall temperature distributions on the flat plate have been obtained for small nozzle-to-plate distances.

The results show that the interaction of shock waves in the freejet with a plate shock formed in front of the impingement plate depends strongly on the distance of the plate from the nozzle exit. Consequently, the surface pressure and adiabatic wall temperature distributions on the impinging plate are changed significantly with the nozzle-to-plate distance. The temperature recovery on the plate, where a supersonic jet impinges, is characterized by 1) the consistent existence of a cooled region near the jet periphery and 2) the central cooled region that appears occasionally. The former is due to the vortex-induced total temperature separation, and the latter is mainly attributable to the vortex–shock interaction. However, the surface pressure distribution, which has the peripheral maximum, implies that the cooling in the central region is linked with the existence of a stagnation bubble: The cooling effect in the central region may be enhanced by the stagnation bubble, which traps the fluids with a lowered total temperature.

For the inclined jet impingement, the maximum surface pressure increases as the impinging angle decreases, and the peak is displaced

slightly from the geometric center of the plate to the upward region. From the pressure profile, the stagnation bubble is expected to disappear, and the cooling effect in the central region is conspicuously weakened: The recovery factor in the central region for this configuration is over 0.95. Therefore, it confirms that the stagnation bubble contributes to enhancement of the cooling effect in the central region.

Acknowledgments

This research was supported by Ministry of Science and Technology through their National Research Laboratory program and by the Agency for Defence Development, Contract UD000012AD.

References

[1]Kalghatgi, G. T., and Hunt, B. L., "The Occurrence of Stagnation Bubbles in Supersonic Impingement Flows," *Aeronautical Quarterly*, Vol. 27, No. 3, 1976, pp. 169–185.

[2]Gummer, J. H., and Hunt, B. L., "The Impingement of a Uniform, Axisymmetric, Supersonic Jet on a Perpendicular Flat Plate," *Aeronautical Quarterly*, Vol. 22, 1971, pp. 403–420.

[3]Donaldson, C. D., and Snedeker, R. S., "A Study of Free Jet Impingement. Part 1. Mean Properties of Free and Impinging Jets," *Journal of Fluid Mechanics*, Vol. 45, Pt. 2, 1971, pp. 281–319.

[4]Donaldson, C. D., Snedeker, R. S., and Margolis, D. P., "A Study of Free Jet Impingement. Part 2. Free Jet Turbulent Structure and Impingement Heat Transfer," *Journal of Fluid Mechanics*, Vol. 45, Pt. 3, 1971, pp. 477–512.

[5]Ginzburg, I. P., Semiletenko, B. G., Terpigor'ev, V. S., and Uskov, V. N., "Some Singularities of Supersonic Underexpanded Jet Interaction with a Plane Obstacle," *Journal of Engineering Physics*, Vol. 19, 1973, pp. 1081–1084.

[6]Gubanova, O. I., Lunev, V. V., and Plastina, L. N., "Central Breakaway Zone with Interaction Between a Supersonic Underexpanded Jet and a Barrier," *Fluid Dynamics*, Vol. 6, 1973, pp. 298–301.

[7]Carling, J. C., and Hunt, B. L., "The Near Wall Jet of a Normally Impinging, Uniform, Axisymmetric, Supersonic Jet," *Journal of Fluid Mechanics*, Vol. 66, Pt. 1, 1974, pp. 159–176.

[8]Iwamoto, J., "Impingement of Under-Expanded Jets on a Flat Plate," *Journal of Fluids Engineering*, Vol. 112, No. 2, 1990, pp. 179–184.

[9]Lamont, P. J., and Hunt, B. L., "The Impingement of Underexpanded, Axisymmetric Jets on Perpendicular and Inclined Flat Plates," *Journal of Fluid Mechanics*, Vol. 100, Pt. 3, 1980, pp. 471–511.

[10]Kim, K. H., and Chang, K. S., "Three-Dimensional Structure of a Supersonic Jet Impinging on an Inclined Plate," *Journal of Spacecraft and Rockets*, Vol. 31, No. 5, 1994, pp. 778–782.

[11]Fox, M. D., Kurosaka, M., Hedges, L., and Hirano, K., "The Influence of Vortical Structures on the Thermal Fields of Jets," *Journal of Fluid Mechanics*, Vol. 255, 1993, pp. 447–472.

[12]Fox, M. D., and Kurosaka, M., "Supersonic Cooling by Shock–Vortex Interaction," *Journal of Fluid Mechanics*, Vol. 308, 1996, pp. 363–379.

[13]Abbett, M., "Mach Disk in Underexpanded Exhaust Plumes," *AIAA Journal*, Vol. 9, No. 4, 1971, pp. 512–514.

[14]Back, L. H., and Cuffel, R. F., "Detection of Oblique Shocks in a Conical Nozzle with a Circular-Arc Throat," *AIAA Journal*, Vol. 4, No. 12, 1966, pp. 2219–2221.

[15]Kline, S. J., and McClintock, F. A., "Describing Uncertainties in Single Sample Experiments," *Mechanical Engineering*, Vol. 75, No. 1, 1953, pp. 3–8.